FUDMA International Journal of Social Sciences (FUDIJOSS)
Volume 3 No.2, June 2023
ISSN: 2735-9522 (Print) ISSN: 2735-9530 (Online)

APPLICATION OF ARTIFICIAL NEURAL NETWORK IN FORECASTING LAND SURFACE TEMPERATURE IN KARU LGA, NIGERIA

Danbaba Goma[1], Salihu Abdullahi Chado[2] and Martins Rakiya Ruth[3]
[1&3]Department of Environmental Management, Faculty of Environmental sciences, Bingham University, Kodape-Karu: danbaba.goma@binghamuni.edu.ng or danbaba.goma@gmail.com08067045111; [2]Department of Environmental Management, Faculty of Environmental Sciences, Nigerian Army University, Biu.
*Corresponding Author's E-mail:danbaba.goma@binghamuni.edu.ng

ABSTRACT
Land Surface Temperature (LST) is a significant factor in the relationship between regional microclimatic changes and other environmental factors. This study aims to look at the LST's intensity during three time periods (2002, 2012, and 2022). Second, to predict the LST in Karu, Nigeria, for the years 2032 and 2042. The analysis used geospatial technology and an artificial neural network (ANN). On all maps, LST intensity was depicted. These classifications were based on a +3°C temperature rise within a range of 25°C to > 37°C. The results obtained signifies that classified LST for 2002 revealed a larger portion of area had surface temperature within the ranges of 28° - 31°C and 31° - 34°C covering 52.77% and 36.75% of the total study area. From 2012 and 2022; surface temperature within the range of 28° - 34°C found to dominate the spatial extent of the study area. The rise in urban areas and decline in vegetation cover may be related to this. As a result, an incremental tendency towards high LST being dominant throughout the research area's geographical extent was realised. By 2032 and 2042, 46% of Karu is expected to see temperature increases more than 38°C, following the LST trend. The study's findings confirm that ANN models are effective and capable of forecasting LST while taking into account a variety of characteristics for dynamic and complex real-world datasets. To reduce the occurrence of Urban Heat Islands (UHI) in the area, the research suggested sustainable urban development and increasing plant cover.

Keywords: Artificial Neural Network, Forecast, Karu, Land Surface Temperature, Land-Use/Landcover

Background of the Study
In a mixed urban environment, the concept of land surface temperature (LST) is utilized to interpret the change in land use/land cover (LULC) pattern (Saha *et al.*, 2021; Guha *et al.*, 2020). LST is the surface temperature felt during an exchange of turbulent heat fluxes and long-wave radiation between the land and the atmosphere (Tomlinson *et al.*, 2011). LST was established in several major global cities (including Beijing, Shanghai and Chicago) to address a variety of environmental issues (Das and Das, 2020; Mukherjee and Singh, 2020; Peng *et al.*, 2020).

Changes in urban land use is becoming noticeable in many cities across the world, not only in developed countries but also in African cities due to population growth. According to United Nations Revision of urbanization Prospects Report (2018), the urban population will upsurge by more than 2.5 billion people by 2050, with Asia and Africa accounting for 90 % of the increase, and this is most responsible for changes in urban land surface temperatures witnessed in recent years (Ayanlade, 2017; Masoudi and Tan, 2019; Zhang and Sun, 2019).

A combination of factors has been reported in the literature as the drivers of changes in LST which include the removal of vegetation within urban areas (Ayanlade, 2016), change in urban thermal and physical properties of construction materials, building, morphology, surface roughness (Litardo, *et al.*, 2020), and anthropogenic heat sources modify the local energy and urbanization, leading to increases in atmospheric temperature in urban areas compared to their surroundings (Zhou and Chen, 2018; Aghamohammadi, *et al.*, 2021). Many of these studies concluded that the main causes of the recent intensification of LST in urban areas can be related to structural and land cover differences of urban and rural areas. Urban areas are rough with buildings extending above ground level and are dry and impervious with construction materials extending across natural soils and vegetation. These urban characteristics alter the natural surface energy and radiation balances such that urban areas are relatively warm places (Kabano, Lindley and Harris, 2021). Therefore, the rapid population growth rate is speedily increasing and significantly impacting LULC in different parts of the world (Kafy *et. al.*, 2021; Naim and. Kafy, 2021). The change in LULC substantially affects the ecosystem and biodiversity, which significantly increases the LST and accelerates climate change risks (Kafy *et al.*, 2021).

In addition, the LULC transformation progressively contributes to the arrangement of a warmer thermal condition resulting in creating the Urban Heat Island (UHI) effect (Dey *et al.*, 2021). The UHI phenomenon harms social aspects, public health, and ecological sustainability (Fu and Weng, 2018). Thus, the changes in LULC and LST are necessary to assess in order to achieve systematic urban growth with a proper land use management plan for ensuring environmental sustainability at the city and regional level (Nurwanda and Honjo, 2020; Faisal *et al.*, 2021).

The application of Remote Sensing (RS) and the Geographic Information System (GIS) have provided opportunities to estimate LULC changes and the LST distribution in a particular region (Kafy, *et.al.* 2021). In Nigeria, several studies like (Maduako, *et al.*, 2016; Maduako, Yun, and Patrick, 2016; Ayanlade, Aigbiremolen and Oladosu, 2021) have described the LULC change and its impacts on LST using multi-temporal Landsat images, Selective satellite images like Thermal Infra-Red Sensors (TIRS) and Artificial Neural Network (ANN) were used to identify and predict the LULC and LST. Furthermore, because UHI and LST have a close relationship, several studies like (Mas and Flores, 2008; Ahmed, *et. al.*, 2013; Wang *et al.*, 2017; Sheik-Mujabar, 2019) have assessed these two using the Remote Sensing database.

Other methods and algorithms, Markov Chain (MC) (Halmy *et. al.*, 2015). Cellular Automata (CA) (Ozturk, 2015; Al-sharif and Pradhan, 2015) and Logistic Regression (LR) (Arsanjani, *et al.*, 2013), were used to predict the LULC and LST changes in several studies. Every method consists of its own strength and limitations. If variations in land cover were known, but there is no geographical dependence and distribution, the MC is preferred for the prediction (Halmy, *et. al.*, 2015). Depending on the prior position of cells in a region, the CA model specifies the position of cells in an array, according to a set of transition laws (Balogun and Ishola, 2017). The CA model is widely used for potential LULC simulation and predicts the future LULC change matrix by incorporating the past pattern of change (Yang *et. al.*, 2012). The main advantage of this model is that, it focuses on historical trends and driving variables at a distance to highways, slope, and elevation (Ahmed *et. al.*, 2013).

FUDMA International Journal of Social Sciences (FUDIJOSS)
Volume 3 No.2, June 2023
ISSN: 2735-9522 (Print) ISSN: 2735-9530 (Online)

Kappa coefficient values verify the consistency of the CA model (Losiri *et. al.*, 2016). For LST prediction, the ANN concept is extensively used by researchers, which was first established to understand the dynamics of the human brain and its mechanisms (Civco, 1993; Shatnawi and Abu-Qdais, 2019; Rakib *et. al.*, 2020).

The ANN approach does not need any earlier information about the components, and the dynamic structure produces the basic process inside the framework to predict the future LST (Bodri and Cermak, 2003). The multi-layered perceptron (MLP) model, which offers automated judgements for the efficient representation of network parameters, is the foundation upon which the ANN is built. It examines the input and generates a random output with a low to high level of accuracy when it notices a pattern of changes in its neighbouring pixels. The LST can be predicted using a variety of helpful parameters, including latitude, longitude, and LULC maps, Normalised Difference Built-up Index (NDBI), Normalised Difference Bare Soil Index (NDBSI), and Normalised Difference Vegetation Index (NDVI). The NDBI and NDBSI are significantly more significant characteristics than the NDVI, which is a lesser predictor of LST. If complicated and non-linear correlations are found, one of the ANN's most significant benefits is its capacity to represent them (Yao, 1999). The ANN does not place limitations on input parameters, unlike any other prediction model (Van-Gerven and Bohte, 2017). The best fitting model to use for LST imitation is ANN since hypothesis-oriented indicators cannot match with historical trends (Nurwanda and Honjo, 2020).

Numerous models that deal with LST prediction exist, including Multivariate Adaptive Regression Splines (MARS), Wavelength Neural Networks (WNN), Adaptive Neuro-Fuzzy Interference Systems (ANFIS), and Dynamic Evolving Neuro-Fuzzy Inference Systems (DENFIS), but Artificial Neural Networks (ANNs) are a potent tool that uses a machine learning algorithm to model complex behaviour. Since ANNs are independent from the relationships in the input data, unlike the majority of multi-variate modelling techniques, there is no need to make any assumptions about the spatial autocorrelation and multi-collinearity of the data. Previous research by (Lee and Lathrop, 2006; Díaz-Robles *et al.*, 2008; Triantakonstantis and Stathakis, 2015; Rahman *and Rifaat,* 2021) has found-out that LST is largely dependent on LULC. Therefore, prediction of LULC for evaluating future change in LST is needed in Karu Local Government Area in Nasarawa State, Nigeria.

Karu Local Government Area like many other settlements around the Federal Capital Territory (FCT) Abuja is experiencing tremendous urban transformation since the last decade and rapid rate of urbanization. The study area in recent time has experience massive LULC changes and serious apprehensions related to thermal discomfort and heat related issues making it a suitable location for study as these issues affect more than 333,800 thousand residents (Nasarawa State, 2021), which form the fulcrum of this paper. Therefore, this paper's two goals are as follows: First, to investigate the variation in land surface temperature throughout three time periods (2002, 2012, and 2022). The second step is to model the LST in order to predict future LST. This study's contribution to LST modelling aims to enhance suitable decision-making processes and offer a valuable tool for sustainable urban design.

FUDMA International Journal of Social Sciences (FUDIJOSS)
Volume 3 No.2, June 2023
ISSN: 2735-9522 (Print) ISSN: 2735-9530 (Online)

Materials and Methods

Study Area

Nasarawa State's Karu Local Government Area is situated between longitudes 7°54'E and 9°25'E of the Greenwich Meridian and latitudes 8°5'N or 10°42'N (Figure 1). In October 1991, the Local Government was established. The Nigerian Federal Capital Territory is not far from Karu. As a result of its shared borders with Abuja to the west, Keffi LGA in Nasarawa State to the south, and Jaba LGA in Kaduna State to the north, the major towns of Karu are included in the Federal Capital Territory's population development corridors. Karu is an unplanned region with a geographic size of around 2,640 KM^2 (Karu Area Urban Plan and Development Authority) (KAPDA, 2001; Udeh, 2010).

Figure 1: Study Area map of Karu LGA

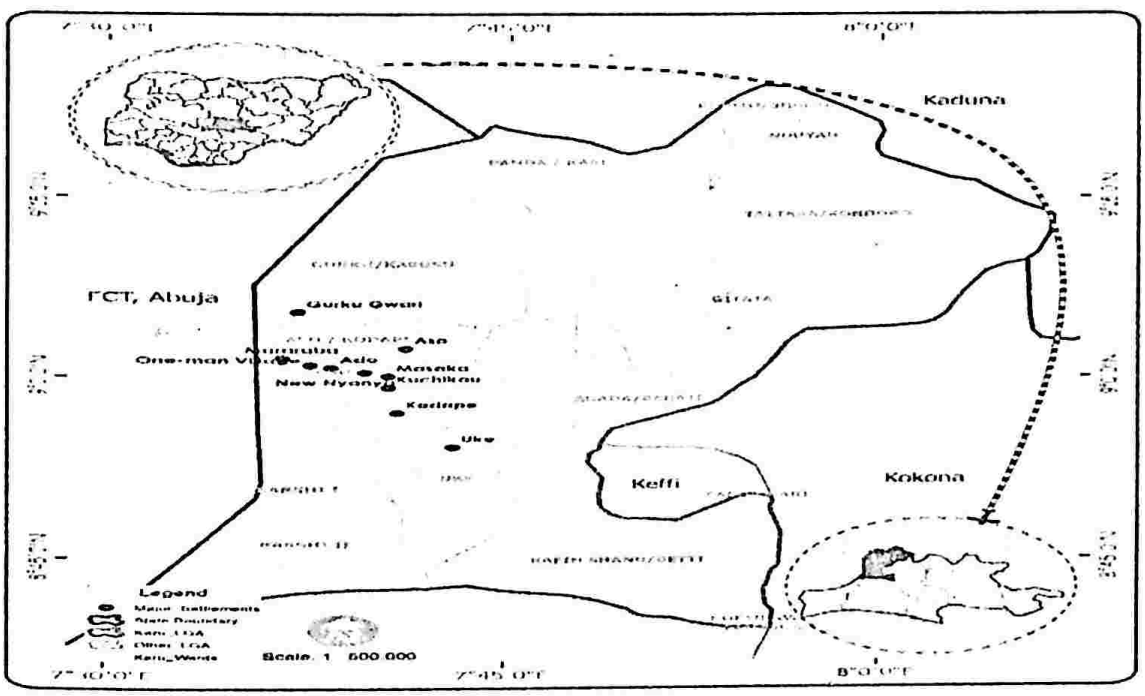

Source: Adapted from Administrative Map of Nasarawa State.

The area has a population of 10,000 in 1991, and is believed to have grown rapidly to 216,230 by 2006 (NPC, 2009) (due to the continuous migration and influx of people from other parts of the country to this area (Udeh, 2010). Its current population is estimated at 333,800 (via a growth rate of 3.7% annually) (Nasarawa State Ministry of Lands and Survey, 2022) Karu's climate is distinguished by a dry season from November to March and a wet season from April to October. The rainy season lasts anywhere from 180 to 190 days. The average annual rainfall is 1,632mm, with the most falling in July, August, and September (Nasarawa State, 2021). Karu's greatest temperature is recorded during the dry season, when there is little to no cloud cover. The yearly temperature ranges from 210°C to 370°C (Nasarawa State, 2021). The maximum temperature is lower during the rainy season due to extensive cloud cover, and the diurnal yearly range is also substantially lower, sometimes not

FUDMA International Journal of Social Sciences (FUDIJOSS)
Volume 3 No.2, June 2023
ISSN: 2735-9522 (Print) ISSN: 2735-9530 (Online)

exceeding 70 degrees Celsius in July and August. At higher elevations during the dry season, relative humidity is around 20%, whereas it is 30% at lower elevations. It may reach 90% in the morning and 50% in the afternoon during the wet season. The oppressive in terms of decreased comfort level in the valleys and plains (Udeh, 2010).Karu is home to a significant network of rivers and streams, many of which are little and ephemeral. The major rivers, the Ado and Uke, flow continuously. According to Udeh (2010), the native vegetation is of the park savannah variety and consists of dense tropical woods with shrubs and grasses.

Data Collection

Various spatial analyses were performed for Karu LGA. Of which, Landsat 8 OLI and 7 TM data were derived from available sources (United States Geological Survey -USGS- Earth Explorer) and was downloaded at the epochs of November, March and April (i.e., to get the best cloud free image); 2002, 2012 and 2022. For the analysis, aster's digital elevation model was also downloaded and extracted. Information about the satellite images used as sources for this study's analysis is shown in Table 1.

Table 1: Sourced Satellite Imagery

Date of Acquisition	Satellite Data	Sensor	Band No.	Spectral range (Wavelength μm)	Spatial Resolution (m)
21/11/2002	Landsat 7	TM	1	0.45–0.52	30
			2	0.52–0.60	30
			3	0.63–0.69	30
			4	0.76–0.90	30
			6	10.4012.50	120 resampled to 30
16/02/2012	Landsat 7	TM	1	0.45–0.52	30
			2	0.52–0.60	30
			3	0.63–0.69	30
			4	0.76–0.90	30
			5	1.551.75	30
			6	10.4012.50	120 resampled to 30
05/02/2022	Landsat 8	OLI	2	0.45–0.51	30
			3	0.64–0.67	30
			4	0.53–0.59	30
			5	0.85–0.88	30
			6	1.57–1.65	30
		TRIS 1	10	10.60–11.19	100 resampled to 30
		TRIS 2	11	11.50–12.51	100 resampled to 30
10/02/2022	DEM	SRTM	---	---	1 Arc

Source: Researcher's Compilation, 2023

Methods of Data Analysis

Land cover, NDVI, and LST calculations were made in order using the downloaded data. The data was used to calculate and reclassify parameters that are anticipated to have an impact on future LST. LST was anticipated to last 20 years. Following that, a comparison of scatter plots, a correlation analysis, and a quantitative and qualitative evaluation of the anticipated LST were noted. The flow diagram (Figure 2) depicts the entire methodological approach.

FUDMA International Journal of Social Sciences (FUDIJOSS)
Volume 3 No.2, June 2023
ISSN: 2735-9522 (Print) ISSN: 2735-9530 (Online)

Figure 2: Methodological Approach

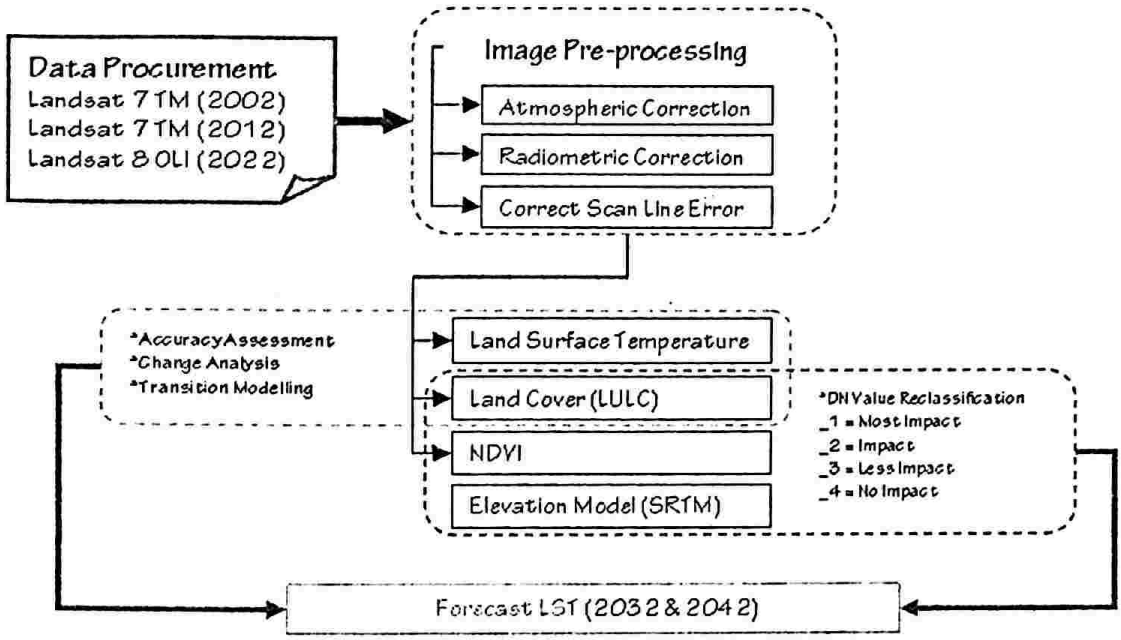

Source: Researcher's Compilation, 2023

Image Pre-processing and Analysis

Datasets were masked using the clip boundary function of ESRI's ArcGIS 10.2.2 software for Karu LGA. Atmospheric and Radiometric corrections were carried out on both Landsat 7 and 8 which were the downloaded satellite imagery. Scan line error correction was also performed on Landsat 7 TM imagery obtained to enhance resolution for analysis. Satellite images obtained were combined and True Color Composite (TCC) was created using appropriate band combinations for all images to enable the creation of training samples and identify the various LULC classes (Good and Giordano, 2019). Maximum Likelihood Supervised Classification (MLSC) approach was used to categorize Landsat Images into four major LULC classes (built-up area, barren terrain, shrub land, and dense vegetation) for the years 2002, 2012 and 2022. For each LULC class, a total of 30 samples were collected to create LULC maps. Each categorized map has been assessed for accuracy using user and producer accuracy, and kappa index (Pontius and Millones, 2011). Based on the fact that the National Aeronautics and Space Administration's (NASA) ASTER Global Digital Elevation Map (version 2) had a spatial resolution of 30m by 30m, elevation data was made available. To get a working spatial resolution of 100m x 100m, the dataset was resample. Additionally, the slope map was created using these elevation data.

FUDMA International Journal of Social Sciences (FUDIJOSS)
Volume 3 No.2, June 2023
ISSN: 2735-9522 (Print) ISSN: 2735-9530 (Online)

Land Surface Temperature (LST)

i. Conversion to Top Atmosphere (TOA) Radiance: using the radiance rescaling factor, Thermal infra-red digital numbers were converted to TOA spectral radiance using equation 1a for Landsat 7 TM data and 1b for Landsat 8 OLI data (Liu and Zhang, 2011).

$$L\lambda = \left(\frac{(Lmax - Lmin)}{(QCALmax - QCALmin)}\right) \times (QCAL - QCALmin) + Lmin\lambda \quad - \quad - \quad \text{-(1a) \_Landsat 7 TM}$$

$$L\lambda = M_L \times Q_{cal} + A_L \quad - \quad - \quad - \quad \text{- (1b) \_Landsat 8 OLI}$$

Where:

$L\lambda$ = TOA spectral radiance (Watts / (m^2 * sr * μm)
M_L = Radiance Multiplicative Band
A_L = Radiance Add Band
Q_{cal} = Quantized and calibrated standard product pixel values
O_I = Correction value for Band 10 is 0.29

ii. Conversion to Top of Atmosphere (TOA) Brightness Temperature (BT): Utilising the thermal constant values from the downloaded Landsat metadata file, the spectrum of the thermal infrared band was converted to active radiance sensor brightness temperature. −273.15 which was added to the equation to enable temperature unit conversion from Kelvin (K) to Celsius Degrees (°C) (Rahman *et al.*, 2017; Sholihah and Shibata, 2019).

$$BT = \left(\frac{K2}{\ln\left(K1/L\lambda\right)} + 1\right) - 273.15 \quad - \quad - \quad - \quad \text{- (2) \_Landsat 7 \& 8}$$

Where:

BT = Top of Atmosphere temperature
$L\lambda$ = TOA spectral radiance (Watts / (m^2 * sr * μm)
$K1$ = K1 constant Band
$K2$ = K2 Constant Band

The value of K1 and K2 for Landsat 7 and Landsat 8 are given as follow as shown in Table 2 (Liu and Zhang, 2011).

Table 2: Calibration Constants for Landsat Thermal Bands

Constant	Unit K1: W/(m^2×sr×μm)	Unit K2: Kelvin
Landsat 7 TM	666.09	1282.71
Landsat 8 OLI TRIS (Band 10)	774.8853	1221.0789
Landsat 8 OLI TRIS (Band 11)	480.8883	1201.1442

Source: Researcher's Compilation, 2023

iii.Normalized Difference Vegetation Indices (NDVI): The Normalized Differential Vegetation Index (NDVI) is a standard vegetation index which is calculated using Near Infra-red and Red respectively. Several scholars have demonstrated that the surface emissivity is highly correlated with the NDVI, and so the emissivity can be calculated using the NDVI (Ahmed *et al.*, 2013). See equation (3).

$$NDVI = \frac{NIR - RED}{NIR + RED} \quad - \quad - \quad - \quad \text{- (3) \_Landsat 8 OLI}$$

Where:

RED = DN Values from the RED Band
NIR = DN Values from the Near Infra-red band

FUDMA International Journal of Social Sciences (FUDIJOSS)
Volume 3 No.2, June 2023
ISSN: 2735-9522 (Print) ISSN: 2735-9530 (Online)

Vi. Land Surface Emissivity (LSE): The average emissivity of a component of the earth's surface is measured as land surface emissivity (LSE), which is derived from NDVI data. The aforementioned correction can be achieved by calculating the land surface spectral emissivity (Ɛ). Meanwhile, some elements such as water content, chemical composition, structure, and roughness all affect the emissivity of the surface (Zine-El -Abidine *et al.*, 2014). See equation (4 and 5).

$$PV = \left(\frac{NDVI - NDVI_{min}}{NDVI_{max} - NDVI_{min}}\right)^2 \quad - \quad - \quad - \quad -(4)\_\text{Landsat 8 OLI}$$

Where:
PV = Proportion of Vegetation
$NDVI$ = DN values from NDVI Image
$NDVI_{min}$ = Minimum DN value from NDVI image
$NDVI_{max}$ = Maximum DN value from NDVI image

$$Ɛ = 0.004 \times PV + 0.986 \quad - \quad - \quad - \quad -(5)\_\text{Landsat 8 OLI}$$

Where:
Ɛ = Land Surface Emissivity
PV = Land Surface Vegetation
0.986 corresponds to a correction value of the equation

v. Land Surface Temperature:The LST is the radiative temperature which was calculated using Top of Atmosphere brightness temperature, wavelength of emitted radiance, Land Surface Emissivity via the following equation 6 (Zine-El-Abidine *et al.*, 2014).

$$LST = \frac{BT}{\left(1 + \lambda \times \left(\frac{BT}{C_2}\right) \times \ln(E)\right)} \quad - \quad - \quad - \quad -(6)\_\text{Landsat 8 OLI}$$

Here, C_2 = 143888 um k or 14380
Where:
BT = Top of atmosphere brightness temperature (Centigrade C)
λ = wavelength of emitted radiance
E = Land surface Emissivity
$C2$ $= h \times {}^{c}/_{\sigma}$ - - - - - - - - - - - - - -(7)
$= 1.4388 \times 10^{-2} mk$
$= 14388\ mk$
h = Planck's constant = $(6.626 \times 10^{-34}$ Js)
c = velocity of light = $(2.998 \times 10^{8}$ ms$^{-2})$
σ = Boltzmann constant = 5.67×10^{-8} Wm^{2}k^{-4} = $(1.38 \times 10^{-23}$ JK)

3.4 Land Surface Temperature Transitional Drivers

Elevation data, NDVI, and Land Cover Classification are the LST transitional drivers that were incorporated into the ANN model (Figure 3). These drivers were reclassified into four categorical values ranging from 1 – 4 (1 = Most Impact, 2 = Moderate Impact, 3 = Less Impact, and 4 = No Impact). This is to depict the intensity of impact each variable has on transitioning LST (Pal and Ziaul, 2017)

Land Surface Temperature Transition and Forecast Model

Using artificial neural networks, the transition model offers the potential for transition from high LST to low LST. Haven provided the transitional driving variables and Quantum Geographic Information System (QGIS) 10.18.2's Modules for Land Use Changes Evaluation (MOLUSCE) plugin extension was used to produce a transitional potential map. In order to

FUDMA International Journal of Social Sciences (FUDIJOSS)
Volume 3 No.2, June 2023
ISSN: 2735-9522 (Print) ISSN: 2735-9530 (Online)

produce a more accurate representation of the data being modelled, the model itself determines how the drivers evolve. Under an iterative framework procedure, the model achieves maximum accuracy (Eastman, 2012). Figure 3 depicts the architecture of the LST prediction model.

Figure 3: Adopted LST Forecast Model Architecture

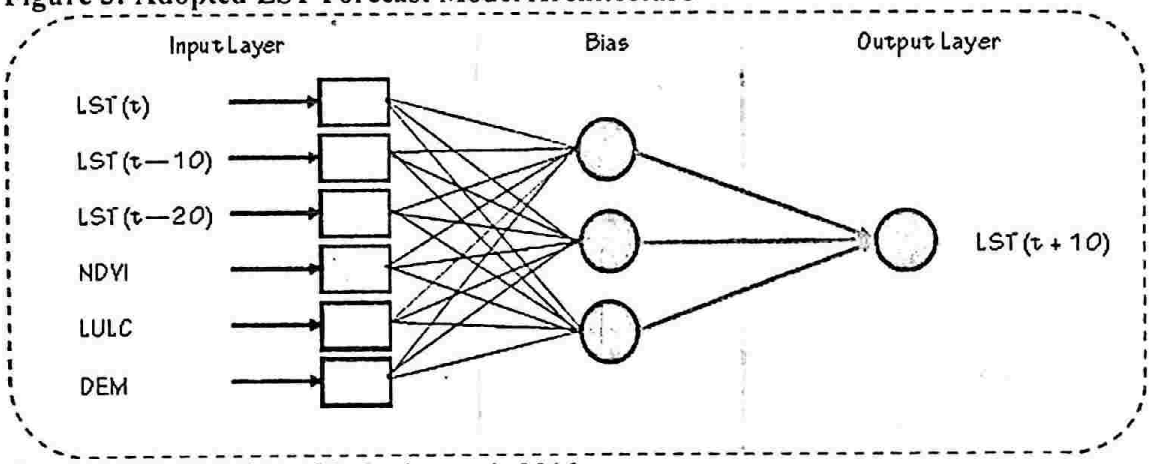

Source: Adopted from Maduako *et al.*, 2016.

Shannon's entropy model

Researchers have used the methods to measure urban sprawl with the help of the Geographic Information System (GIS) (Dhali *et al.*, 2019; Kumar *et al.* 2020). The entropy model has calculated this using the following formula.

$$H_n = \sum_{i=1}^{n} P_i log_e\left(\frac{1}{P_i}\right) \text{ - } 8$$

Where, Pi indicates the proportion of phenomenon occurring in the □h zone $\left(P_i - \frac{X_i}{\sum_{i=1}^{n} X_i}\right)$ is the observed value occurring in the □h zone. n denote the total number of zones. The value range of entropy model is from 0 to log_e (n). 0 value indicates that the urban built-up area is vary compact where log_e (n) denotes that the built-up area distribution is dispersed. The scale of relative entropy value is the range of 0 to 1. The relative entropy (Hi) for n number of zones can be calculated in this formula $H_n^1 = \frac{H_n}{log_e(n)}$. - - - - - - - - - - -9

Where n denote the number of zones for urban sprawling study. The eight areas were established for calculating the urban sprawling areas namely, Mararaba, Ado, New Nyanya, Masaka, Aso, Uke, Kuchikau and Kodape.

Results and Discussion

Land Use Land Cover Analysis

The total land area for the study was 2,640km². The categorized imagery for 2002 revealed a larger portion of area were occupied by dense vegetation 1114.80km² which represents 42.23% of the total land. In 2012 it decreased to 677.74km² which accounts for 25.67% of the total area and in 2022 it was lowered up to 188.82km² which represents 7.15% of the total area. Low level of urban growth and few other technological activities needed to convert vegetation land to built-up area for human settlement, commercial and other forms of agricultural land usage. This finding is similar to that of Hammad *et al.* (2018) in the

FUDMA International Journal of Social Sciences (FUDIJOSS)
Volume 3 No.2, June 2023
ISSN: 2735-9522 (Print) ISSN: 2735-9530 (Online)

Southern Syria coastal basin where vegetation area decreased from about 64% in 1987 to about 38% in 2017. In 2002 shrub occupied 913.76km² which represents 34.61% of the total land. The progressive significant increase continued up till 2012 which occupied 1197.42km² and accounted for 45.36% of the total land but in 2022, it slightly declined to 1110.82km² which constituted 42.07% of the total land area. In 2002 bare land constituted 519.99km² which accounted for 19.70% and progressively increased from 655.63km² which represented 24.83% in 2012 to 1102.47km² which accounted for 41.76% in 2022. In 2002 built area occupied 91.45km² which represented 3.46% and continue to increase from 109.20km² which constituted 4.14% in 2012 to 237.89km² which accounted for 9.01% in 2022 (See Figures 4, 5 and 6).

Figure 4: Classified land use land cover map of the study area in 2002

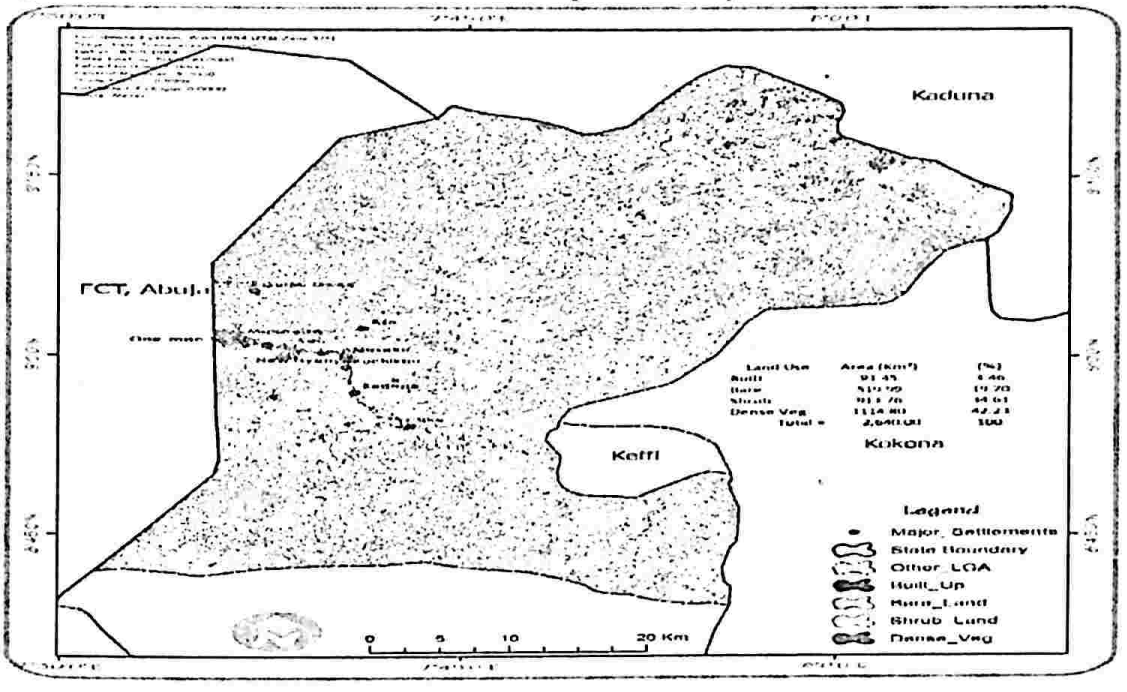

Source: Researcher's Analysis, 2023

FUDMA International Journal of Social Sciences (FUDIJOSS)
Volume 3 No.2, June 2023
ISSN: 2735-9522 (Print) ISSN: 2735-9530 (Online)

Figure 5: Classified land use land cover map of the study area in 2012

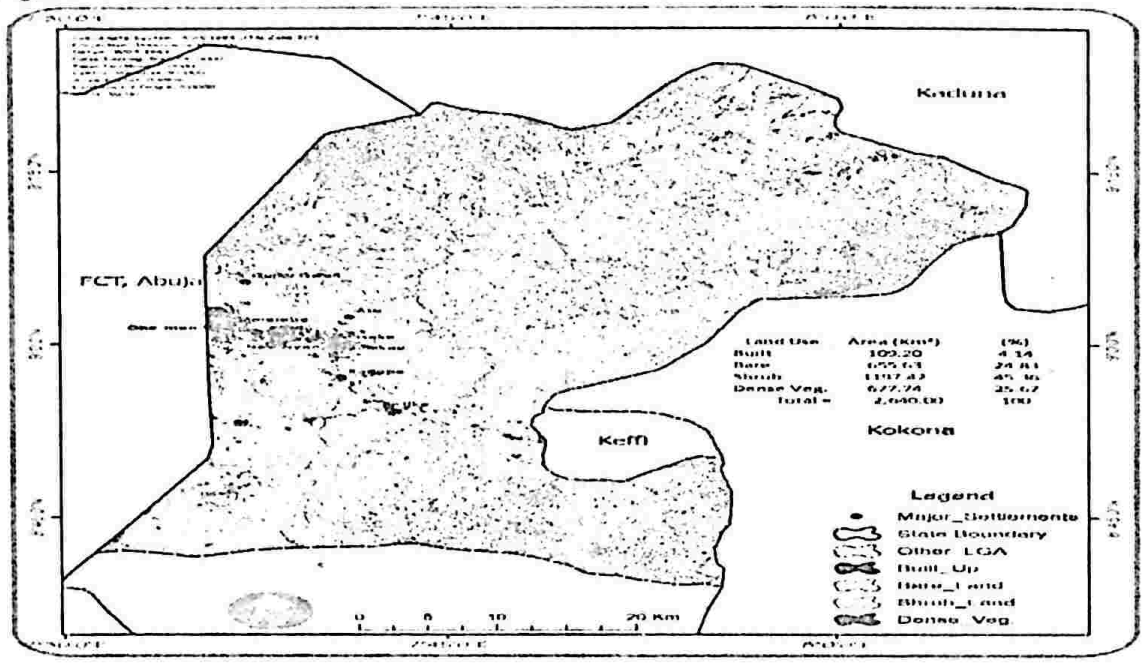

Source: Researcher's Analysis, 2023

Figure 6: Classified land use land cover map of the study area in 2022

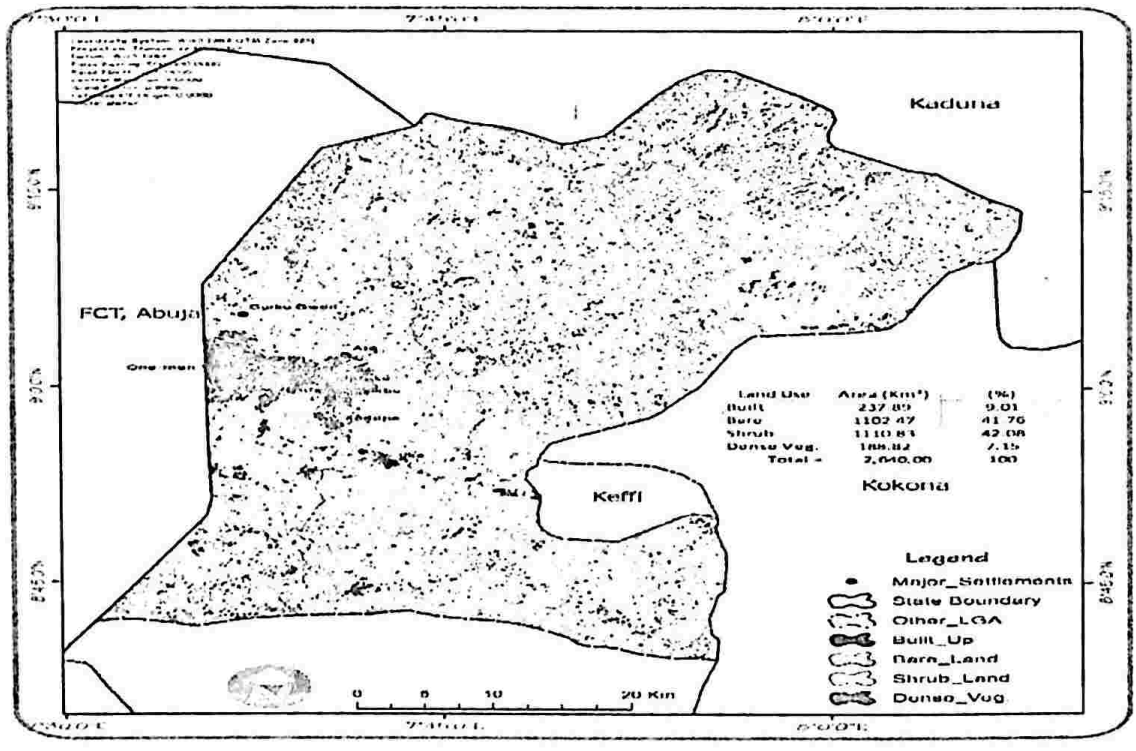

Source: Researcher's Analysis, 2023

FUDMA International Journal of Social Sciences (FUDIJOSS)
Volume 3 No.2, June 2023
ISSN: 2735-9522 (Print) ISSN: 2735-9530 (Online)

Table 3: Change Analysis for LULC in the study area from 2002 to 2022

Land Use	Area in km²			Change in %	
	2002	2012	2022	Δ 2002 _ 2012	Δ 2012 _ 2022
Built-up areas	91.45	109.20	237.89	0.67	4.87
Baren terrain	519.99	655.63	1102.47	5.14	16.93
Shrub land	913.76	1197.42	1110.82	10.74	-3.28
Dense Vegetation	1114.80	677.74	188.82	-16.56	-18.52
Total =	2,640	2,640	2.640		

Source: Researcher's Analysis, 2023 ΔPercentage Change

An important aspect of change detection is to determine what is actually changing. The major changes that occurred between the periods of 2002 and 2012 were mainly evident in the decrease in dense vegetation. Vegetation loss to other LULC categories was -16.56km². The net rate of change between 2012 and 2022 shows that the different land use types such as dense vegetation and shrub have a negative loss change. Danse vegetation rate of loss is -18.52km² and shrub is -3.28km². It can be noticed during the period under consideration that, dense vegetation and rock shrub LULC lost their land in favour of bare and built land. All these are negative changes that enabled bare-land to gain 16.93km² and built 4.87km² (Table 3). Vegetation land was the most affected and this has implication on the climatic condition in the study area. Comparing the LULC results from 2002, 2012, and 2022 allowed for the calculation of the percentage change in each land cover class over time. The amount of vegetated land declined significantly by 18.53 percent between 2012 and 2022. The built-up area increased by 4.87% of the entire study area during the same time period (see Table 3).

Deforestation, urban sprawl, and other human activities like agricultural practises have significantly changed the climatic conditions and fragmented the vegetal cover of the planet. Vegetation provides many ecosystem services, including removing carbon dioxide from the atmosphere, reducing soil erosion, and preventing flooding. Important ecosystem services will be altered or destroyed when forest areas are converted to built-up area. The result also substantiates the finding of Oyinloye (2013) who asserted that the direct relationship between rapid urban growth and commercial centers, industrial centers, tourism resorts and population influx has a basis from land use changes. The reduction in vegetation decreased the amount of oxygen in the air, which worsened the effects of the problem associated to urban heat islands over the study area.

LULC Accuracy Assessment

30 sampling sites were compared with the equivalent point on Google Earth pictures taken during the same time period in order to validate the land use classification. Whereas, the validation, the Kappa coefficient statistics, and the overall classification accuracy all demonstrated good accuracy.

FUDMA International Journal of Social Sciences (FUDIJOSS)
Volume 3 No.2, June 2023
ISSN: 2735-9522 (Print) ISSN: 2735-9530 (Online)

Table 4: Accuracy Assessment for LULC Classification

	2002 (%)	2012 (%)	2022 (%)
Overall Accuracy	83.33	81.31	86.67
Kappa Coefficient	77.74	78.38	82.20

Source: Researcher's Analysis, 2023.

The accuracy level is classified as very strong when the Kappa coefficient is greater than 0.75 (Congalton and Green, 2008; Foody, 2002). Table 4 shows the classification of overall accuracy and the land use classification Kappa coefficient as a result. The total accuracy for the years 2002, 2012, and 2022 was 83.33%, 81.31%, and 86.67%, respectively; the corresponding Kappa coefficients were 77.74%, 78.38%, and 82.20%. The results are in tandem with Kappa coefficient values (above 0.75) which indicate that the LULC data produced by the MLSC procedure has a high enough accuracy to be useful for analyzing LULC and identifying changes (Mondal *et al.*, 2016).

Land Surface Temperature (LST)

The spatial pattern of LST distribution calculated for this study was well represented by Figure(s) 7, 8 and 9. LST intensity was represented in all maps using a color spectrum of dark blue (depicting low temperature) to dark red (depicting high surface temperature) within 6 classified ranges. These classified ranges were based on an increment of +3°C within a spectrum of < 25°C to > 37°C.

Figure 7: Classified LST map of the study area in 2002

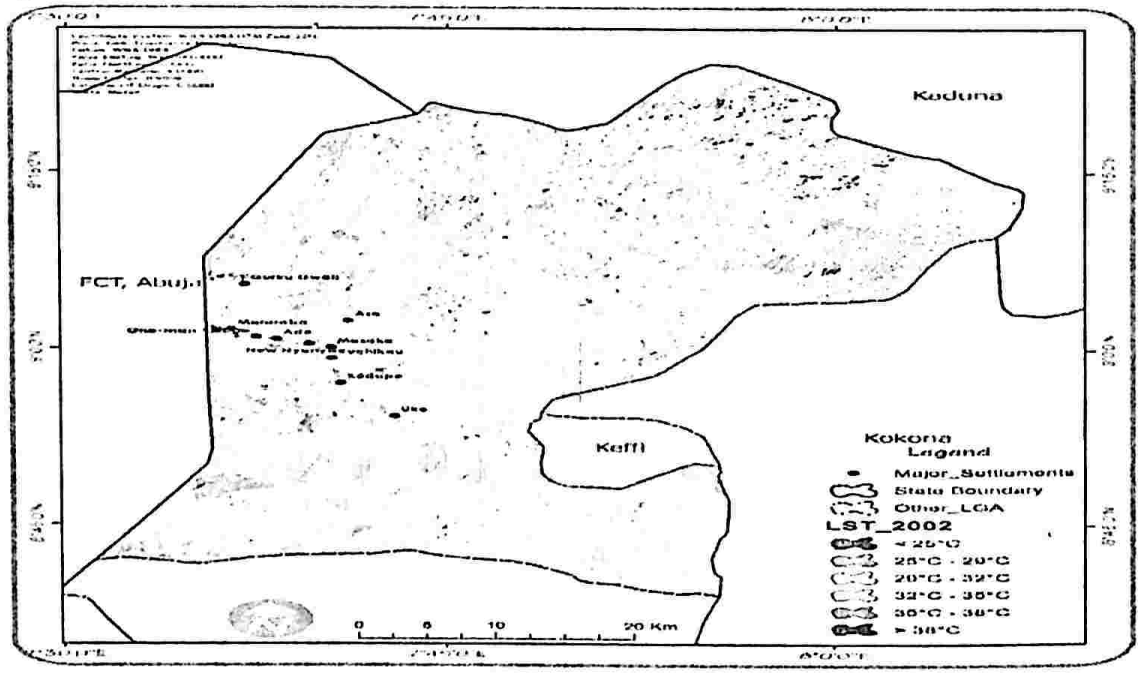

Source: Researcher's Analysis, 2023

FUDMA International Journal of Social Sciences (FUDIJOSS)
Volume 3 No.2, June 2023
ISSN: 2735-9522 (Print) ISSN: 2735-9530 (Online)

Figure 8: Classified LST map of the study area in 2012

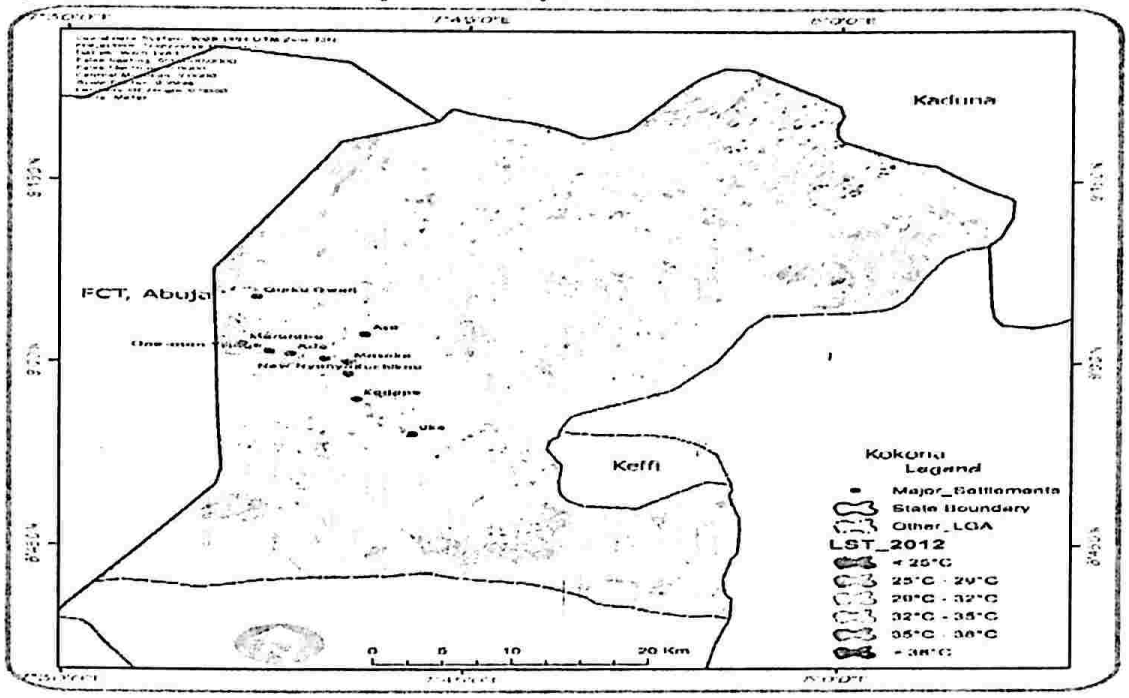

Source: Researcher's Analysis, 2023

Figure 9: Classified LST map of the study area in 2022

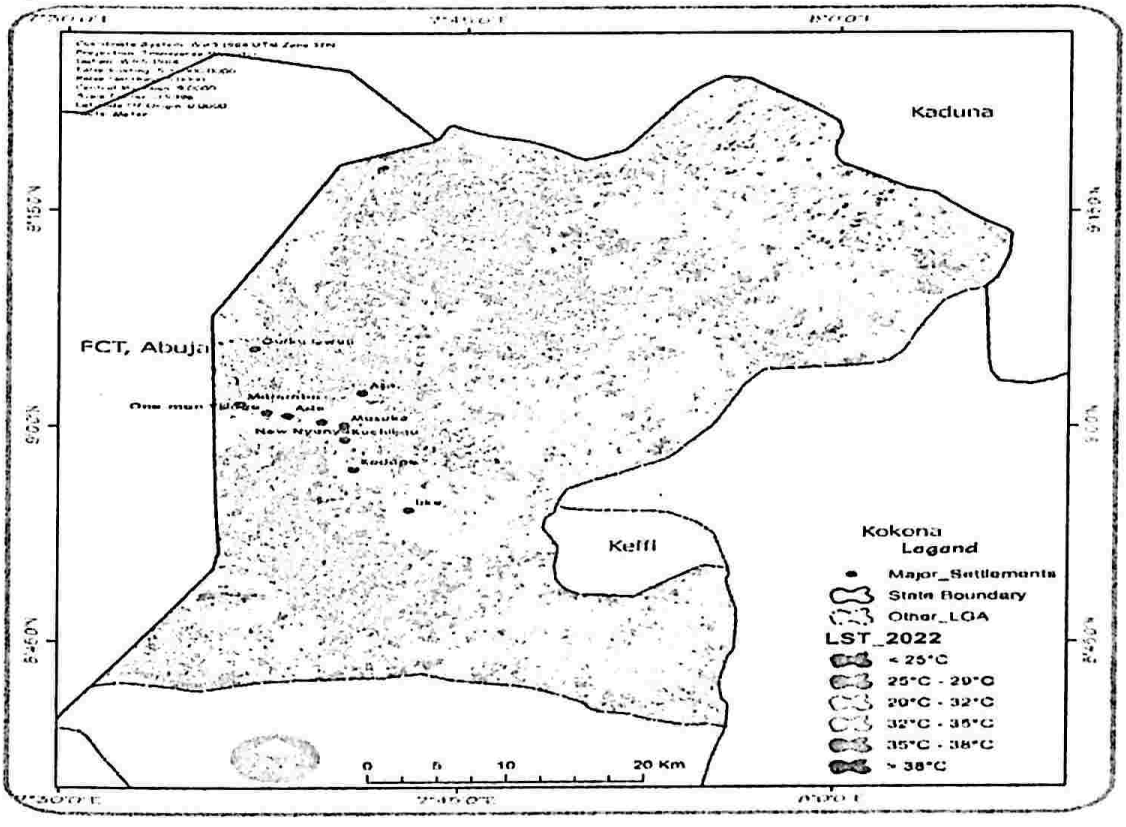

Source: Researcher's Analysis, 2023

FUDMA International Journal of Social Sciences (FUDIJOSS)
Volume 3 No.2, June 2023
ISSN: 2735-9522 (Print) ISSN: 2735-9530 (Online)

Land Surface Temperature Change/Transition Analysis

To give a clearer understanding of the temperature variance at various LST ranges, percentage change in LST was used. Whereas, the categorised LST for 2002 showed that a greater percentage of the region had surface temperatures between 28° and 31°C and 31° and 34°C, respectively, covering 52.77% and 36.75% of the entire research area. Only 7.44% and 0.054% of the entire land surface recorded temperatures between 25° and 28°C and less than 25°C, respectively. Hence, LST greater than 37°C was identified to cover 0.42% of the total area of study for the year 2002. In 2012, LST within the range of 28° - 31°C and 31° - 34°C accounted for 57.47% and 32.59 spatial extent of the study area respectively. Only 7.94% and 0.041% of the spatial trend is within the range of 25° -28°C and <25°C. Consequently, LST identified to be within 34° -37°C represented 1.89% and greater than >37°C is 0.071% of the spatial trend. From 2022, LST is within the range of 31°-34°C which accounted for 59.15% and 34° -37°C which constituted 28.08% of the study area respectively.

Figure 10: LST spatial trend analysis in the study area from 2002 to 2022

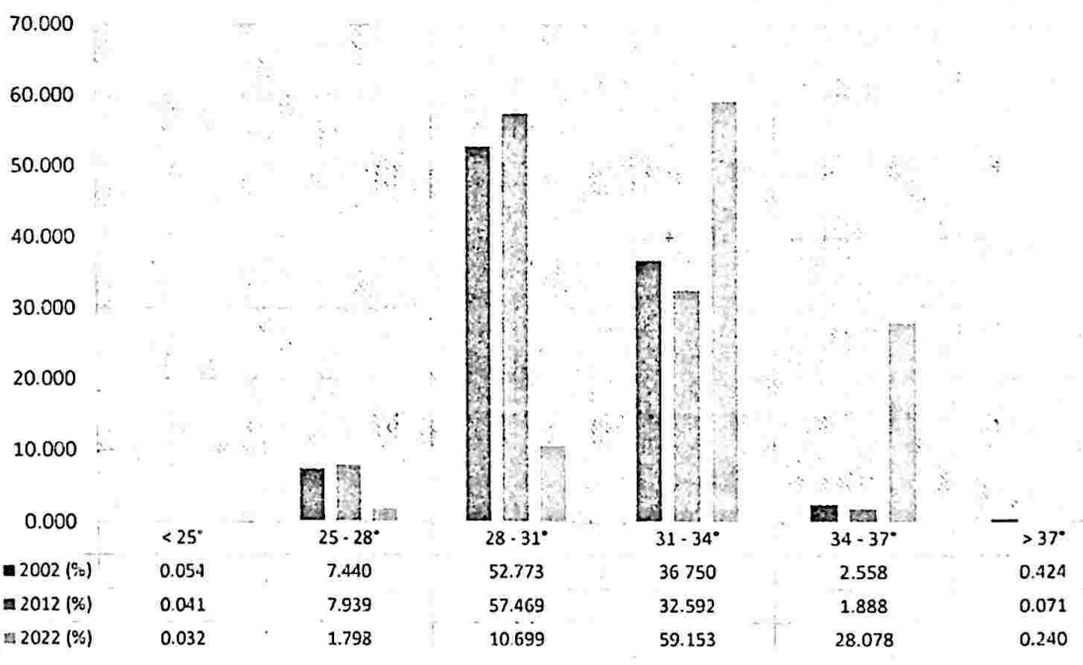

Source: Researcher's Analysis, 2023

According to Table 5 and Figure 1, the change analysis for the LST for the years 2002 to 2012 showed that when the surface temperature was between 250 and 280 degrees Celsius and 280 and 310 degrees Celsius, respectively, they respectively accounted for 0.499% and 4.696% of the positive change in the LST in the study area, but from the range of 250C, 310 to 340 degrees Celsius, 340 to 370 degrees Celsius, and >37 degrees Celsius all have negative LST change in the study area independently.

FUDMA International Journal of Social Sciences (FUDIJOSS)
Volume 3 No.2, June 2023
ISSN: 2735-9522 (Print) ISSN: 2735-9530 (Online)

Table 5: Change Analysis for LST in the study area from 2002 to 2022

LST Range	Area in km²			Change in %	
	2002	2012	2022	Δ 2002 – 2012	Δ 2012 – 2022
< 25°	0.68	1.17	0.94	-0.013	-0.008
25 - 28°	215.35	228.87	51.84	0.499	-6.142
28 - 31°	1521.33	1656.7	308.58	4.696	-46.770
31 - 34°	1059.41	939.54	1706.04	-4.158	26.561
34 - 37°	73.75	54.44	809.81	-0.670	26.190
> 37°	12.23	2.04	6.91	-0.354	0.169
Total =	2882.75	2882.76	2884.12		

Source: Researcher's Analysis, 2023 Δ Percentage Change

Figure 11: LST transitional spatial gain and loss analysis in the study area from 2002 to 2022

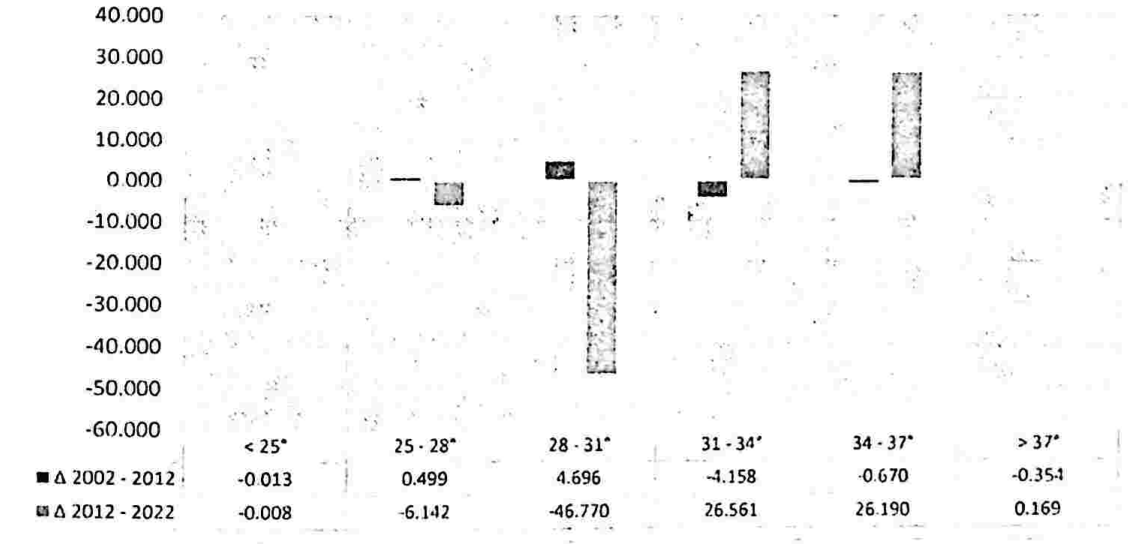

Source: Researcher's Analysis, 2023

Land Surface Temperature Forecast for 2032 and 2042

ANNs are autonomous from the relationships in the input data, unlike most multi-variate modeling techniques; the study did not make any forecasts about spatial autocorrelation or multi-collinearity (Triantakonstantis and Stathakis, 2015). A good agreement of accuracy can be seen when the percentage of correctness is over 80%. With 81.46% correctness and a total Kappa co-efficient value of 0.843, the simulated outcome demonstrated a significant agreement, confirming the accuracy of the ANN model's forecast for 2022 (Table 6).

FUDMA International Journal of Social Sciences (FUDIJOSS)
Volume 3 No.2, June 2023
ISSN: 2735-9522 (Print) ISSN: 2735-9530 (Online)

Table 6: ANN Model validation for LST prediction via QGIS MOLUSCE plugin

Model Validation	2022
% Correctness	81.46
Kappa Coefficient	0.843
Kappa Location	0.818
Kappa-histo	0.831

Source: Researcher's Analysis, 2023

Figures 11 and 12 show LST raster maps for 2022 that show strong agreement in terms of how closely values on the maps match values observed and forecasted. These positive LST 2022 predictions led to the network's projection of LST scenarios for 2032 and 2042 are depicted in Figures 13 and 14.

Figure 12: Forecasted LST map of the study area for the year 2032

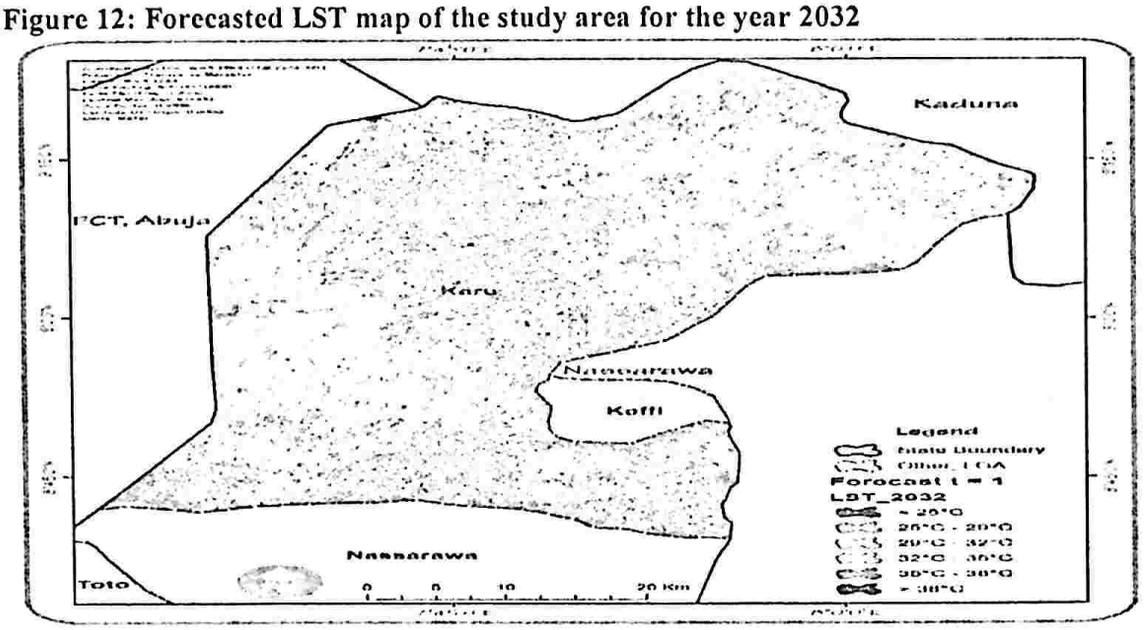

Source: Researcher's Analysis, 2023

FUDMA International Journal of Social Sciences (FUDIJOSS)
Volume 3 No.2, June 2023
ISSN: 2735-9522 (Print) ISSN: 2735-9530 (Online)

Figure 13: Forecasted LST map of the study area for the year 2042

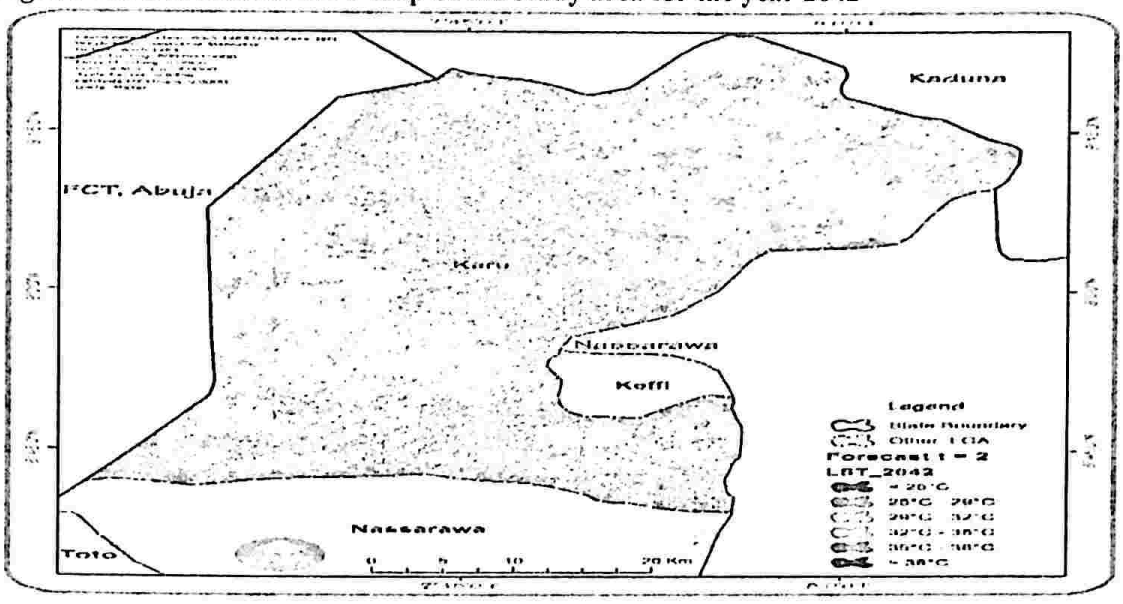

Source: Researcher's Analysis, 2023

Based on the rate of change in Table 5 between 2002 and 2022, the forecast change in table 6, revealed that by 2032, surface temperature will increase slightly from 1706.04km^2 in 2022 at LST range of 31° -34°C to 1879.09km^2 in 2032 and 809.81km^2 at LST range 34° -37°C to 923.84km^2.

The LST will increase from 68.54km2 in 2032 to 108.67km2 in 2042 in a temperature range of 280 - 310C. Utilising ANN and correlation approaches, the study predicted the LST in response to the LULC. Over Karu, it is clear that urbanisation has changed the LULC. These

LULC modifications have a bearing on the UHI-causing urban thermal environment. The research area's built-up land expanded as a result of the decreased vegetation cover. The results also show that there was a considerable temperature difference between the metropolitan core and the surrounding areas. Similar results have been found by earlier researchers who have also looked into this topic (Feng et al., 2018; Halder and Bandyopadhyay, 2021; Hassan et al., 2021). However, this problem can be lessened by enhancing forest cover and water bodies, as well as through sustainable development.

Table 6: Change Analysis for observed forecasted LST in the study area, 2022 to 042

LST Range	Area in km²			Change in %	
	2022	2032	2042	Δ 2022 – 2032	Δ 2032 – 2042
< 25°	0.94	0.29	0.05	-0.65	-0.24
25 - 28°	51.84	6.24	0.71	-45.6	-5.53
28 - 31°	308.58	68.54	108.67	-240.04	40.13
31 - 34°	1706.04	1879.09	1862.64	173.05	-16.45
34 - 37°	809.81	923.84	909.19	114.03	-14.65
> 37°	6.91	6.23	2.96	-0.68	-3.27
Total =	2884.12	2884.23	2884.22		

Source: Researcher's Analysis (2023). Δ Percentage Change

FUDMA International Journal of Social Sciences (FUDIJOSS)
Volume 3 No.2, June 2023
ISSN: 2735-9522 (Print) ISSN: 2735-9530 (Online)

Analysis of urban growth using Shannon's entropy model

Due to urban growth, the built-up area is the area of this site that is most impacted. Due to the rapid rate of urbanisation over the past 20 years, the eight quadrants were utilised to determine the built-up developing over the land usage (Table 7). In 2002, the built-up rate is high in the Mararaba, Ado, and Masaka areas. After that, Mararaba areas have more built-up expansion in the year 2012. According to the map of 2022, there are more developed areas in Mararaba, Aso, Ado, and New Nyanya.

Karu LGA. has become one of the fastest growing urban areas in Nigeria. It has an annual growth rate of over 40% owing to the rapid rate of urban growth and economic development principally as a result of the influx of migrants from other parts of the country (Muhammad, *et al.* 2022). The findings indicate that the last twenty years have seen an increase of the entire built-up region. Shannon various time intervals are used to improve entropy levels. The fact that the entropy score is below 1 indicates that towns are adopting compact urban expansion gradually between 2002 and 2022.

Table 7: Quadrant-wise and Overall Distribution of Shannon's Entropy Value (2002–2022).

Years	*Quadrants*								*Overall En Value*
	Mararaba	Ado	New Nyanya	Masaka	Aso	Uke	Kuchikau	Kodape	
2002	0.28	0.24	0.22	0.24	0.22	0.20	0.20	0.20	0.34
2012	0.40	0.26	0.24	0.22	0.28	0.24	0.20	0.20	0.40
2022	0.48	0.34	0.34	0.30	0.38	0.28	0.28	0.24	0.48

Source: Researcher's Analysis, 2023.

Conclusion

The study investigated the use of an artificial neural network (ANN) to forecast LST values from a series of past years' values over a 20-year period (2002-2022) and projected to 2042. The study has further confirmed that the ANN model can anticipate LST with accuracy. These classifications were based on a +3°C temperature rise within a range of 25°C to > 37°C. The data show that a larger section of the area had surface temperatures between 28° and 31°C and 31° and 34°C, respectively, representing 52.77% and 36.75% of the entire research area. Only 7.44% and 0.054% of the entire land surface recorded temperatures between 25° and 28°C and less than 25°C, respectively. Hence, LST greater than 37°C was identified to cover 0.42% of the total area of study for the year 2002. From 2012 and 2022; surface temperature within the range of 28 – 34 was found to dominate the spatial extent of the study area.

Urban Heat Island (UHIs) is a bad trend for Karu LGA because it is a factor contributing to the microclimatic warming that is currently occurring in the study area; if nothing is done to mitigate this trend in LST intensification, the study area may experience severe UHI, which will have a negative impact on Karu's livelihoods. Also, following the LST trend, 46% of Karu is forecasted to have increased temperatures greater than 38°C by 2032 and 2042. The outcome of the study reaffirms the efficiency and capability of ANN models to forecast LST considering various parameters for the complex and dynamic real-world datasets. The paper recommends that, Urban planners and local administrators should emphasize sustainable

urban development that will reduce the effect of UHI and encourage the establishment of parks and open space to serve as shelter-belt for ecological stability.

Reference

Aghamohammadi, N., Ramakreshnan, L., Fong, C. S. and Sulaiman, N. M., (2021) Urban Heat Island, Contributing Factors, Public Responses and Mitigation Approaches in the Tropical Context of Malaysia. *Urban Heat Island Mitigat. 2021, 107–121.*

Ahmed, B. Kamruzzaman, M., Zhu, X., Rahman, M.S. and Choi, K. (2013). Simulating Land Cover Changes and their Impacts on Land Surface Temperature in Dhaka, Bangladesh, *Rem. Sens. 5 5969–5998.*

Al-sharif, A.A. and Pradhan, B. (2015). A Novel Approach for Predicting the Spatial Patterns of Urban Expansion by Combining the Chi-squared Automatic Integration Detection Decision Tree, Markov Chain and Cellular Automata Models in GIS, *Geocarto Int. 30 858–881.*

Arsanjani, J.J., Helbich, M., Kainz, W. and Boloorani, A.D. (2013). Integration of Logistic Regression, Markov Chain and Cellular Automata Models to Simulate Urban Expansion, *Int. J. Appl. Earth Obs. Geoinf. 21 265–275.*

Ayanlade, A. (2016). Variation in Diurnal and Seasonal Urban Land Surface Temperature: Land-use Change Impacts Assessment over Lagos metropolitan city. Model. *Earth Syst. Environ. 2, 193.*

Ayanlade, A. (2017).Variations in Urban Surface Temperature: An Assessment of Land Use Change Impacts over Lagos Metropolis. *Weather 72, 315–319.*

Ayanlade, A., Aigbiremolen M.I and Oladosu, O.R., (2021). Variations in Urban Land Surface Temperature Intensity over Four Cities in Different Ecological Zones. *Journal of Scientific Report 11: 20537*

Balogun, I. and Ishola, K. (2017). Projection of Future Changes in Land-Use/Land-Cover Using Cellular Automata/Markov Model over Akure City, Nigeria, *J. Remote Sens. Technol. 5 22–31.*

Bodri, L. and Cermak, V. (2003). Prediction of Surface Air Temperatures by Neural Network, Example Based on Three-year Temperature Monitoring at Sporilov Station, *Studies Geophys. Geod. 47 173–184.*

Civco, D.L. (1993). Artificial Neural Networks for Land-Cover Classification and Mapping, *Int. J. Geogr. Inf. Sci. 7 173–186.*

Congalton R. and Green K. (2008). Assessing the Accuracy of Remotely Sensed Data: Principles and Practices. Second Edition, CRC Press Boca Raton.

Das M. and Das A. (2020). Urban Climate Assessing the Relationship Between Local Climatic zones and Land Surface Temperature – A case study of Sriniketan-Santiniketan Planning Area, West Bengal, India. *Urban Climate, 32*

Dey, N.N, Al-Rakib, A., Kafy, A.A., Raikwar, V. (2021). Geospatial Modelling of Changes in LULC Dynamics Using Multi-Layer Perception Markov Chain Model in Rajshahi City, Bangladesh, Environmental Challenges, 100148.

Diaz-Robles L. A., Ortega J. C., Fu J. S., Reed G. D., and Chow J. C., (2008) "A Hybrid ARIMA and Artificial Neural Networks Model to Forecast Particulate Matter in Urban Areas: The Case of Temuco, Chile," *Atmospheric Environment, 42(35), 8331-8340.*

Dhali, M. K., Chakraborty, M., and Sahana, M. (2019). Assessing Spatio-temporal Growth of Urban Sub-Centre Using Shannon's Entropy Model and Principal Component Analysis: Lower Ganga River Basin, India. *The Egyptian Journal of Remote Sensing and Space Science, 22(1), 25-35.*

Eastman J. R. (2012), Idrisi Selva Manual. Clark University, *Worcester, 324.*

Faisal, A.A., Kafy, A.A., Al-Rakib, A., Akter, K.S., Raikwar, V. and Jahir D.M.A (2021). Assessment and Prediction of Seasonal LST Change Using Multi-Temporal Landsat Images and Their Impacts on Agricultural Yields in Rajshahi, Bangladesh, *Environmental Challenges*, 100147.

Feng, Y., Li H., Tony, X., Chen, L. and Liu, Y. (2018) 'Projection of Land Surface Temperature Considering the Effects of Future Land Change in the Taihu Lake Basin of China', *Global and Planetary Change, 167, 24–34.*

Foody G.M. (2002). Status of Land Cover Classification Accuracy Assessment. *Remote Sensing and Environment 80 185-201.*

Fu, P. and Weng, Q. (2018). Responses of Urban Heat Island in Atlanta to Different Land-Use Scenarios, *Theor. Appl. Climatol. 133 123–135.*

Good, T. and Giordano, P. A. (2019). Methods for Constructing a Color Composite Image. In: Google Patents.

Guha S., Govil H., Gill N. and Dey A. (2020). Analytical Study on the Relationship Between LST and LULC *indices. Annals of GIS, 26(2), 201–216.*

Halder, B. and Bandyopadhyay, J. (2021) 'Evaluating the Impact of Climate Change on Urban Environment Using Geospatial Technologies in the Planning Area of Bilaspur, India', *Environmental Challenges, 5, 100286.*

Halmy, M.W.A. Gessler, P.E., Hicke, J.A. and Salem, B.B. (2015). LULC Change Detection and Prediction in the North-Western Coastal Desert of Egypt Using Markov CA, *Appl. Geogr. 63 101–112.*

Hammada, M., Mucsi, L. and Van-Leeuwen, B. (2018). Land Cover Change Investigation in the Southern Syrian Coastal Basin during the Past 30-years Using Landsat Remote Sensing Data. *Journal of Environmental Geography* 11(2) 45-51

Hassan, T., Zhang, J., Prodhan, F.A., Sharma, T.P.P. and Bashir, B. (2021) 'Surface Urban Heat Islands Dynamics in Response to LULC and Vegetation Across South Asia (2000–2019)', *Remote Sensing, 13(16), 3177.*

Kabano, P., Lindley, S. and Harris, A. (2021). Evidence of Urban Heat Island Impacts on the Vegetation Growing Season Length in a Tropical city. *Landsc. Urban Plan. 206, 103989.*

Kafy, A. A., Al-Rakib, A., Akter, K.S., Rahaman, Z.A., Faisal A. A. and Mallik, S. (2021). Monitoring the Effects of Vegetation Cover Losses on Land Surface Temperature Dynamics Using Geospatial Approach in Rajshahi City, Bangladesh, *Environmental Challenges*, 100187.

Karu Area Urban Plan and Development Authority (KAPDA), (2001) *Karu Planning Development Area Report.* Nasarawa, Nigeria.

Kumar, J., Biswas, B., and Walker, S. (2020). Multi-temporal LULC Classification Using Hybrid Approach and Monitoring Built-up Growth with Shannon's Entropy for a Semi-arid Region of Rajasthan, India. *Journal of the Geological Society of India, 95(6), 626- 635.*

Lee S. and Lathrop R. G., (2006); "Subpixel Analysis of Landsat ETM+ Using Self-Organizing Map (SOM) Neural Networks for Urban Land Cover Characterization," *IEEE Transactions on Geoscience and Remote Sensing, 44(6), 1642-1654.*

Litardo, J., Palme, M, Borbor-Cordova, M., Caiza, R., Macias, J., Hidalgo-Leon, R. and Soriano, G. (2020). Urban Heat Island Intensity and Buildings' Energy Needs in Duran, Ecuador: Simulation Studies and Proposal of Mitigation Strategies. *Sustainable Cities and Society 62, 102387*

Liu, L. and Zhang, Y. (2011). Urban Heat Island Analysis Using the Landsat TM Data and ASTER Data: A Case Study in Hong Kong. *Remote Sensing, 3(7), 1535-1552.*

Losiri, C., Nagai, M., Ninsawat, S., Shrestha, R.P. (2016). Modelling Urban Expansion in Bangkok Metropolitan Region using Demographic–Economic Data through Cellular Automata-Markov Chain and Multi-Layer Perceptron-Markov Chain Models, *Sustainability 8 686.*

Maduako, I.D., Yun, Z., and Patrick, B. (2016). Simulation and Prediction of Land Surface Temperature (LST) Dynamics within Ikom City in Nigeria using Artificial Neural Network (ANN), *J. Remote Sens. GIS 5 1–7.*

Maduako, I, Elijah, E., Yun Z., and Patrick, B., (2016). Prediction of Land Surface Temperature (LST) Changes within Ikom City in Nigeria Using Artificial Neural Network (ANN). *International Journal of Remote Sensing Applications (IJRSA) Volume 6,*

Mas, J.F. and Flores, J.J. (2008). The Application of Artificial Neural Networks to the Analysis of Remotely Sensed Data, *Int. J. Rem. Sens. 29 617–663.*

Masoudi, M. and Tan, P. Y. (2019). Multi-year Comparison of the Efects of Spatial Pattern of Urban Green Spaces on Urban Land Surface Temperature. *Landsc. Urban Plan. 184, 44–58.*

Mondal, M. S., Sharma, N., Garg, P.K. and Kappas, M. (2016) 'Statistical Independence Test and Validation of CA Markov LULC Prediction Results', *The Egyptian Journal of Remote Sensing and Space Science, 19(2), 259–272.*

Muhammad, I., Ezra, I, Abdulkadir, M. Y., Muhammad, A.T. and Hadiza, T.A. (2022) Urban Growth and Housing Problems in Karu Local Government Area of Nasarawa State, Nigeria. *Global Journal of Research and Review*

Munzi, S., Correia, O., Silva, P. and Lopes, N. (2014) 'Lichens as Ecological Indicators in Urban Areas: Beyond the Effects of Pollutants', *Journal of Applied Ecology, 51(6), 1750–1757.*

Mukherjee F. and Singh D. (2020). Assessing LULC Change and Its Impact on LST Using LANDSAT Data: A Comparison of Two Urban Areas in India. Earth Systems and Environment 2020 4:2, 4(2), 385–407.

Mustafa, E. K. Yungang C.O., Liu, G., Kaloop M.R., Beshr, A.A., Fawzi, Z and Mohammed, S. (2020) 'Study for Predicting LST using Landsat Data: A Comparison of Four Algorithms', *Advances in Civil Engineering, 438.*

Naim, M.N.H and. Kafy, A.A. (2021). Assessment of Urban Thermal Field Variance Index and Defining the Relationship between Land Cover and Surface Temperature in Chattogram City: A Remote Sensing and Statistical Approach, *Environmental Challenges,* 1000.

Nasarawa State, (2021). *Nasarawa State.* Department of Geography and Planning, University of Jos, Nigeria.

Nassarawa State Ministry of Lands and Survey (2022). *Map of Nasarawa State.*

National Population Commission (2009). Federal Republic of Nigeria Official Gazette 24 Vol. 94 Lagos Nigeria

Nurwanda, A. and Honjo, T. (2020). The prediction of City Expansion and Land Surface Temperature in Bogor City, *Indonesia, Sustain. Cities Soc. 52 101.*

Oyinloye, M.A. (2013). Geospatial Analysis of Urban Growth in Akure, Ondo State, Nigeria. *American Journal of Social Issues and Humanities* 3 (4), 200-212

Ozturk, D. (2015). Urban Growth Simulation of Atakum (Samsun, Turkey) using Cellular Automata-Markov Chain and Multi-layer Perceptron-Markov Chain Models, *Rem. Sens. 7 5918–5950.*

Pal, S. and Ziaul, S. (2017). Detection of Land Use and Land Cover Change and Land Surface Temperature in English Bazar Urban Centre, *Egypt. J. Remote Sens. Space Sci. 20 125–145.*

Peng X., Wu W., Zheng Y., Sun J., Hu T. and Wang P. (2020). Correlation Analysis of Land Surface Temperature and Topographic Elements in Hangzhou, China. *Scientific Reports*

Pontius Jr, R. G., and Millones, M. (2011). Death to Kappa: Birth of Quantity Disagreement and Allocation Disagreement for Accuracy Assessment. *International Journal of Remote Sensing, 32(15), 4407-4429.*

Rahman, M., Aldosary, A. S., and Mortoja, M. (2017). Modeling Future Land Cover Changes and their Effects on the LST in the Saudi Arabian Eastern Coastal City of Dammam.*Land, 6(2), 36.*

Rahman M.H. and Rifaat S.M. (2021). Using Spatio-Temporal Deep Learning for Forecasting Demand and Supply Gap in Ride-hailing System with Anonymized Spatial Adjacency Information. *IET Intelligent Transport System 15 941-957.*

Rakib, A.A., Akter, K., Rahman, M.N. Arpi, S. and A. A. Kafy, A. A. (2020). Analyzing the Pattern of Land Use Land Cover Change and its Impact on Land Surface Temperature: Remote Sensing Approach in mymensingh, Bangladesh, in: *1st International Student Research Conference, Dhaka.*

Saha S., Saha A., Das M., Saha A., Sarkar R. and Das A. (2021). Analyzing Spatial Relationship between LULC and LST of Three Urban Agglomerations of Eastern India. Remote Sensing Applications: *Society and Environment, 22*

Shatnawi, N. and Abu-Qdais, H. (2019). Mapping Urban Land Surface Temperature Using Remote Sensing Techniques and Artificial Neural Network Modelling, *Int. J. Rem. Sens. 1–16.*

Sheik-Mujabar P (2019) 'Spatial-Temporal Variation of LST of Jubail Industrial City, Saudi Arabia Due to Seasonal Effect by using Thermal Infrared Remote Sensor Satellite Data', *Journal of African Earth Sciences, 155, 54– 63.*

Sholihah, R. I., and Shibata, S. (2019). *Retrieving Spatial Variation of Land Surface TemperatureBased on Landsat OLI/TIRS of Southern Jember, Java, Indonesia.* Paper presented at the IOP Conference Series: Earth and Environmental Science.

Tomlinson, C. J., Chapman, L., Thornes, J.E. and Baker, C. (2011) 'Remote Sensing Land Surface Temperature for Meteorology and Climatology: A Review', *Meteorological Applications, 18(3), 296–306.*

Triantakonstantis D., and Stathakis D. (2015) Urban Growth Prediction in Athens, Greece, Using Artificial Neural Networks. World Academy of Science, Engineering and Technology *International Journal of Architectural and Environmental Engineering 9, (3).*

Udeh, A.U. (2010) Impact of Development of the Federal Capital City, Abuja on Selected Settlements in Karu Local Government Area, Nasarawa State, Nigeria

United Nations Revision of urbanization Prospects Report (2018). *World Urbanization Prospects Produced* by the Population Division of the United Nations Department of Economic and Social Affairs, USA.

Van Gerven, M. and Bohte, S. (2017). Artificial Neural Networks as Models of Neural Information Processing, Front. *Comput. Neurosci. 11 114.*

Wang, H., Zhang, Y., Tsou, J.Y. and Li, Y. (2017). Surface Urban Heat Island Analysis of Shanghai (China) Based on the Change of Land Use and Land Cover, *Sustainability 9 1538.*

Yang, X., Zheng, X.Q. and Lv, L.N., (2012). A Spatio-temporal Model of Land Use Change Based on ant Colony Optimization, Markov Chain and Cellular Automata, *Ecol. Model. 233 11–19.*

Yao, X. (1999). Evolving Artificial Neural Networks, *Proc. IEEE 87 1423–1447.*

Zhang, Y. and Sun, L. (2019). Spatial-Temporal Impacts of Urban LULC on LST: Case Studies of two Canadian Urban Areas. I*nt. J. Appl. Earth Obs. Geoinf. 75, 171–181.*

Zhou, X. and Chen, H. (2018). Impact of Urbanization-Related LULC Changes and Urban Morphology Changes on the Urban Heat Island Phenomenon. *Sci. Total Environ. 635, 1467–1476.*

Zine El Abidine, E. M., Mohieldeen, Y. E., Mohamed, A. A., Modawi, O.. and Al-Sulaiti, M. H. (2014). Heat Wave Hazard Modelling: Qatar Case Study. *QScience connect, 9.*